Physics – Uspekhi **38** (6) 653 – 664 (1995)

METHODOLOGICAL NOTES PACS numbers: 05.40. + j; 07.60.Ly; 78.66.-w; 77.84.Fa

Regular and quasiregular spectra of disordered layer structures

A V Belinskii ¶

Contents

Abstract. Two examples of problems solvable by statistical optics methods are considered. They are quite clear, they can be interpreted in a transparent manner, and they do not require time-consuming calculations. It is shown how the solution of the first problem — the influence of random variations of the optical thickness of a Fabry – Perot interferometer on its transmission spectra — helps to solve the second problem: the 'mystery' of the experimental spectra of polydomain KDP crystals. These examples may be useful in tackling other statistical problems.

1. Introduction

An analysis of the main stages of the development of modern statistical optics shows that it is now in the stage of rapid growth. This has been helped by the success achieved in mastering the technique of counting single photons, which are 'statistical' simply because of their quantum nature. Such remarkable results have been obtained on this topic that one can speak of a 'quantum explosion' in the last decade. Interesting effects have however been found also in classical statistical optics. I hope that the examples given below can be counted among such interesting effects.

Let us consider a system of resonant components forming a statistical ensemble. The resonance frequencies of the components are random but they do have an average frequency and a finite variance. The excitation of the system is random and in the case of optical excitation it is provided by white light. What is the influence of the random nature of the components on the spectral characteristics of such a system as a whole? Clearly, it loses partly its resonant nature. In the trivial case this diminishes the usefulness of the properties of the system. A typical example is the presence of random defects on mirrors in a Fabry – Perot interferometer [1 – 5]. But, there are situations when such a 'stochastic' softening of a resonance can be of constructive value. One example is the domain structure in a KDP (KH_2PO_4) crystal cooled below the Curie temperature. Until recently, there has been no model capable of explaining the origin of characteristic quasiregular transmission spectra of the crystal recorded experimentally in polarised light [6]. The domain layer thickness in such a crystal varies at random. It will be shown below that strangely enough such disorder results in some regularisation of the spectra, which is manifested by their harmonic modulation. This is the constructive role of randomness, as mentioned above.

In contrast to the majority of problems in statistical optics, which usually require cumbersome calculations, consideration of these two examples from a single standpoint is very transparent and gives interesting results which may prove useful in analysis of other systems of this type.

¶ This author's name is someTimes spelt Belinsky in Western literature.

A V Belinskii Physics Department, M V Lomonosov Moscow State University, Vorob'evy gory, 119899 Moscow.
Fax (7-095) 939 31 13. Tel. (7-095) 143 48 31.
E-mail: postmaster@spr.phys.msu.su

Received 23 November 1994; revision received 31 January 1995
Uspekhi Fizicheskikh Nauk **165** (6) 691 – 702 (1995)
Translated by A Tybulewicz

2. Ideal Fabry – Perot interferometer

An ideal Fabry – Perot interferometer is known to consist of two plane and parallel, partly transmitting, mirrors separated by a gap of optical thickness d (Fig. 1a). It is easiest to describe this interferometer by considering an 'unfolded' diagram, i.e. the consecutive images of one mirror by the other (Fig. 1b).

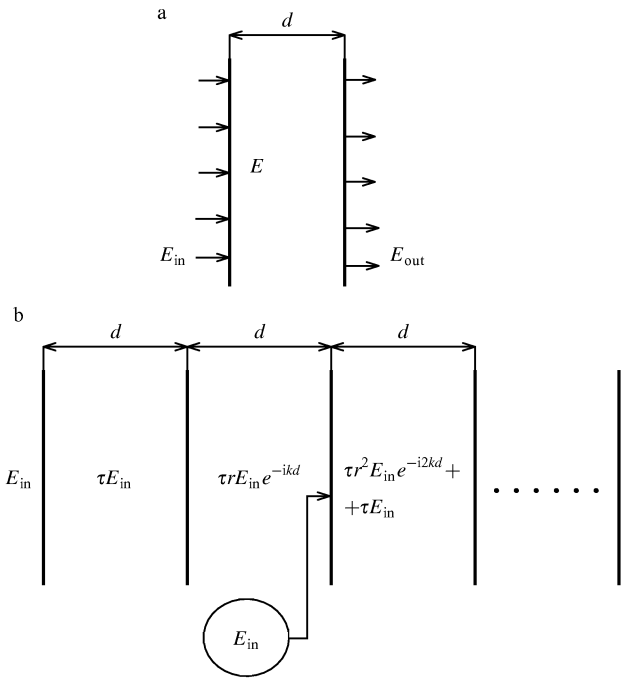

Figure 1. Ideal Fabry–Perot interferometer consisting of two parallel partly transmitting mirrors (a), and its 'unfolded' representation (b). The interferometer is illuminated by a normally incident plane wave with its input amplitude E_{in}. Immediately behind the entry mirror the field amplitude is E and at the exit the output amplitude is E_{out}. The subsequent reflections from the mirrors can be described conveniently by means of the diagram (b).

Let us assume that such an interferometer is illuminated by a parallel beam of rays incident normally on the mirrors. The complex slowly varying amplitude of this beam is E_{in}. The entry mirror transmits radiation of amplitude τE_{in}, where τ is the amplitude transmission coefficient of the mirrors. The beam then acquires a phase delay kd, where $k = 2\pi/\lambda$ is the wave number, and it is reflected from the second mirror (in Fig. 1b it crosses a second plane boundary characterised by an amplitude transmission r, where r is the amplitude reflection coefficient of the mirrors). After a complete round trip of the beam in the interferometer its amplitude is $\tau r^2 \exp(-i2kd) E_{in}$. Reflection from the entry mirror adds to this beam another portion of the illuminating radiation τE_{in} and the cycle is repeated.

The field amplitude inside the interferometer near the entry mirror is thus a sum of the geometric progression

$$E = \tau E_{in} \sum_{n=0}^{\infty} \left[r \exp(-ikd)\right]^{2n} = \frac{\tau E_{in}}{1 - \left[r \exp(-ikd)\right]^2}, \qquad (1)$$

and at the exit from the interferometer the output amplitude is

$$E_{out} = \tau \exp(-ikd) E = \frac{\tau^2 \exp(-ikd) E_{in}}{1 - \left[r \exp(-ikd)\right]^2}. \qquad (2)$$

Therefore, the output intensity of the field is

$$I_{out}(\varphi) = \frac{T^2 I_{in}}{1 - 2R\cos\varphi + R^2}. \qquad (3)$$

where $\varphi = 2kd$ is the phase shift in one round trip of the beam in the interferometer; $T = |\tau|^2$ and $R = |r|^2$ are the intensity transmission and reflection coefficients of the mirrors; in the absence of losses, we have $R + T = 1$. It is assumed that this last condition is always satisfied.

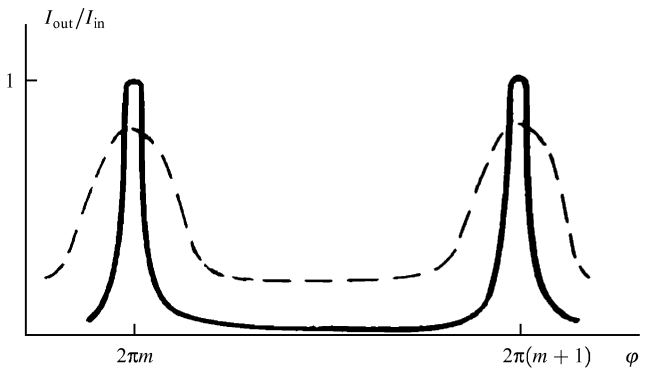

Figure 2. Transmission spectrum of an ideal Fabry–Perot interferometer (continuous curve) and of an interferometer with random Gaussian fluctuations of the thickness (dashed curve).

Expressions (2) and (3) are known as the Airy formulas (see, for example, Ref. [7]). The function (3) represents periodic peaks of unit amplitude. It follows that illumination of this interferometer with white light and an analysis of the spectrum at its exit yields a 'comb' of equidistant fringes (continuous curve in Fig. 2).

3. Geometric-optics model of a Fabry–Perot interferometer with random step defects on mirrors

According to expression (3), the transmission function of a high-quality Fabry–Perot interferometer (i.e. an interferometer with the mirror reflection coefficients R close to unity) is in the form of sharp peaks (Fig. 2). This is evidence of a high sensitivity to a change in the phase φ of a beam travelling between the mirrors. In real situations the mirror fabrication defects and fluctuations of the optical density of the medium filling an interferometer lead to phase shifts, which should be regarded as random. They are related to random changes in the optical thickness d of the interferometer. Errors of this kind can reduce significantly the interferometer quality.

The moments of the distribution of the radiation intensity at the interferometer exit can be described by the following expression for the output intensity:

$$\left\langle I_{out}^n(k) \right\rangle = \int_0^{\infty} I_{out}^n(kd)\, w(d)\, \mathrm{d}d, \qquad (4)$$

where $w(d)$ is the distribution function of the random thickness; $n = 1, 2, \ldots$.

Let us consider the following model of a nonideal interferometer. Let the mirror defects be in the form of steps of random heights and areas (Fig. 3). In the case of normal incidence of the illuminating radiation, such an interferometer can be considered — in the geometric-optics approximation — as a system of ideal interferometers with different optical thicknesses. In the simplest case it is natural to regard the statistics of these interferometers as Gaussian

$$w(\varphi) = \left(\frac{1}{2\pi\sigma^2}\right)^{1/2} \exp\left(-\frac{\varphi^2}{2\sigma^2}\right), \qquad (5)$$

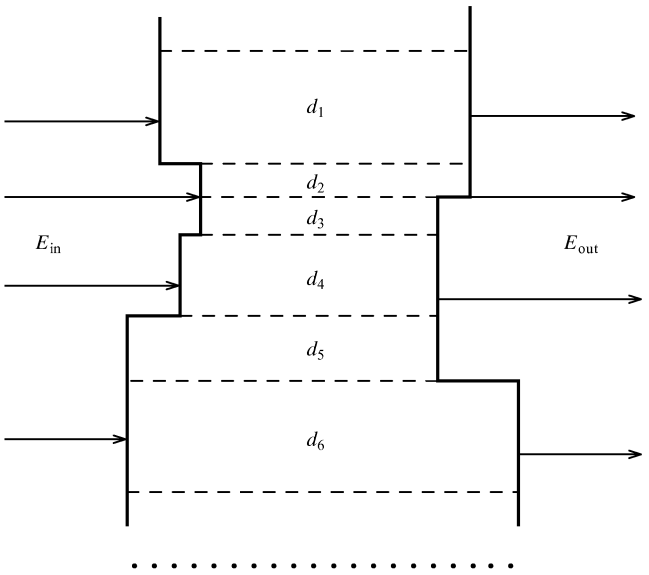

Figure 3. Fabry–Perot interferometer with step defects of the mirrors. The dashed lines identify the ideal, in the geometric-optics approximation, interferometers with constant (but different from one another) thicknesses d_j. These 'microinterferometers' form a statistical ensemble, which represents a real interferometer taken as a whole.

where, for the sake of convenience, the phase fluctuations $\varphi = 2\bar{k}\tilde{d}$ with the variance σ^2 are adopted; $\bar{k}$ is the wave number at some central frequency of the investigated spectrum; $\tilde{d}$ is the fluctuating component of the thickness: $d = \bar{d} + \tilde{d}$, $\langle \tilde{d} \rangle = 0$. In a relatively narrow spectral interval the influence of k on $w(\varphi)$ can be ignored.

This model of the Gaussian statistics of phase fluctuations is justified by the central limit theorem in the theory of probability in the case of uncontrolled random variations of the parameters of the medium and of the interferometer thickness.

The phase shift in one round trip of a wave through the interferometer can be represented in the form

$$2kd = \varphi_{max} + \bar{\varphi} + \varphi\,, \tag{6}$$

where $\varphi_{max} = 2\pi m$ is the phase corresponding to the nearest interference maximum; m is an integer; $|\bar{\varphi}| \leqslant \pi$ is a regular component of the phase deviation from a resonance (from an interference maximum); φ is the fluctuating phase.

The integral given by expression (4), can be calculated, subject to formulas (5) and (6), by approximation of the peaks of the function (3) with the Lorentzian profile:

$$\frac{I_{out}}{I_{in}} = \frac{T^2}{1 - 2R\cos(2kd) + R^2} \equiv \frac{1}{1 + F\sin^2\left[(\bar{\varphi} + \varphi)/2\right]} \cong \frac{1}{1 + F(\bar{\varphi} + \varphi)^2/4}, \tag{7}$$

where $F = 4R/(1-R)^2$ is the fineness factor of an ideal interferometer. This approximation, involving replacement of the sine with its argument, is valid near an interference peak for small values of the phase fluctuations $|\bar{\varphi} + \varphi| \ll 1$. A 'comb' of identical peaks of the function (3) is replaced by one peak. The precision of this approximation improves with the interferometer quality (that is, higher mirror reflection coefficient R and fineness factor F), since a narrow peak corresponds to small phase deviations $\bar{\varphi}$.

It then follows that

$$\frac{\langle I^n_{out}(\bar{\varphi})\rangle}{I^n_{in}} \approx \frac{1}{(2\pi)^{1/2}\sigma}\int_{-\infty}^{\infty} \frac{\exp(-\varphi^2/2\sigma^2)}{\left[1 + F(\bar{\varphi} + \varphi)^2/4\right]^n}\,\mathrm{d}\varphi. \tag{8}$$

The above expression is a convolution of the Gaussian and Lorentzian profiles (for $n = 1$) and it can be calculated analytically, as described in the Appendix. In particular, the first two moments of the output intensity are

$$\langle I_{out}(\bar{\varphi})\rangle = \pi^{1/2} v I_{in}\,\mathrm{Re}\Big\{\left[1 - \mathrm{erf}(v + \mathrm{i}\varphi')\right] \times \exp\left[(v + \mathrm{i}\varphi')^2\right]\Big\}, \tag{9}$$

$$\langle I^2_{out}(\bar{\varphi})\rangle = I^2_{in}\left(v^2 + \pi^{1/2} v\,\mathrm{Re}\Big\{\left[1 - \mathrm{erf}(v + \mathrm{i}\varphi')\right] \times \left[\frac{1}{2} + v(v + \mathrm{i}\varphi')\right]\exp\left[(v + \mathrm{i}\varphi')^2\right]\Big\}\right), \tag{10}$$

where $v = (2/\sigma^2 F)^{1/2}$; $\varphi' = \bar{\varphi}/2^{1/2}\sigma$; $\mathrm{erf}(x) = (2/\pi^{1/2})\int_0^x \exp(-t^2)\,\mathrm{d}t$ is the probability integral (error function).

If the parameters obey $F \gg 1$ and $v \ll 1$, it follows that

$$\langle I_{out}(\bar{\varphi})\rangle \cong I_{in} U^{-1}(\sigma)\exp\left[-\frac{\bar{\varphi}^2}{\varphi_0^2 U^2(\sigma)}\right], \tag{11}$$

where $U(\sigma) = \left[1 + (2\sigma^2 \ln 2)/\varphi_0^2\right]$; $\varphi_0 \cong 2/F^{1/2}$ is the half-width of an interference peak of an ideal interferometer. Consequently, the half-width of a spectral peak of a real interferometer is

$$\varphi_{1/2} \cong \left[\varphi_0^2 + 2\sigma^2 \ln 2\right]^{1/2}. \tag{12}$$

It follows that in the case of an interferometer with Gaussian fluctuations of its thickness the square of the half-width of an interference peak of an ideal interferometer is summed additively with the variance of the phase fluctuations, reduced to the level of 1/2.

A possible form of the spectral transmission function, calculated in accordance with expression (9), is plotted in Fig. 2 (dashed curve). Small fluctuations of the resonance frequencies of the 'microinterferometers' forming a real inter-ferometer do not result in randomisation of the spectral transmission of the system as a whole. They simply 'smooth out' the spectrum reducing its contrast, and they broaden the profiles of the interference maxima. This follows formally from the observation that the transmission function of the system represents, according to expression (8), a convolution of the ideal spectral profile of an interferometer and the distribution function of the random component of the phase shift.

Let us consider one more interesting example of the statistics of steps on the interferometer mirrors. It is interesting not only from the methodological point of view, but also because a formula for the line half-width, similar to formula (12), can be derived in a nontrivial manner.

Let us assume initially that the amplitudes of positive (i.e. those with a positive fluctuating phase shift) and negative steps are the same, and that they produce phase

shifts $\pm\psi$. Then the phase statistics should be similar to the statistics of a random binary signal $\varphi = (-1)^n\psi$ (see, for example, Ref. [8]). Here, $n = n(0, \rho)$ is the number of points at which the average zero value of the phase is crossed (i.e. the number of the mirror steps) in a distance ρ ($n = 0, 1, 2, \ldots$) and which obeys the Poisson law

$$p_n = \frac{(\kappa\rho)^n \exp(-\kappa\rho)}{n!}, \tag{13}$$

where κ is the density of the average number of such zero points per unit length.

An interferometer of this kind thus represents an instrument consisting of two interferometers. In one of them there is a phase shift $\varphi = \psi$ with the probability $p_+ = p_0 + p_2 + \ldots = \exp(-\kappa\rho)\cosh(\kappa\rho)$, whereas in the case of the other interferometer the phase shift is $\varphi = -\psi$ and the probability is $p_- = p_1 + p_3 + \ldots = \exp(-\kappa\rho)\sinh(\kappa\rho)$. Consequently,

$$\langle I_{\text{out}}(\bar{\varphi}, \psi)\rangle = p_+ I_{\text{out}}(\bar{\varphi} + \psi) + p_- I_{\text{out}}(\bar{\varphi} - \psi), \tag{14}$$

where I_{out} with the arguments $\varphi \to \varphi \pm \psi$ is described by expression (3).

Let us now consider fluctuations of the step amplitudes on the assumption, made for the sake of simplicity, that their distribution function is uniform in the interval from 0 to v:

$$;\text{–mm>}\ w(\psi) = \begin{cases} \dfrac{1}{v} & \text{for } 0 \leqslant \psi \leqslant v, \\ 0 & \text{for } \psi > v. \end{cases} \tag{15}$$

Averaging of expression (14) over the distribution (15) gives

$$\langle I_{\text{out}}(\bar{\varphi})\rangle = (v^2G)^{-1/2}\left\{\arctan\left[G^{1/2}\tan\left(\frac{v+\bar{\varphi}}{2}\right)\right] + \arctan\left[G^{1/2}\tan\left(\frac{v-\bar{\varphi}}{2}\right)\right]\right\}, \tag{16}$$

where

$$G = \left(\frac{1+R}{1-R}\right)^2 \cong F. \tag{17}$$

For low values of v and $\bar{\varphi}$, we have

$$\langle I_{\text{out}}(\bar{\varphi})\rangle \cong (v^2G)^{-1/2}\left[\arctan\left(\frac{vG^{1/2}}{1 - G(v^2 - \bar{\varphi}^2)/4}\right) + \delta\pi\right], \tag{18}$$

where

$$\delta = \begin{cases} 0 & \text{for } G\dfrac{v^2 - \bar{\varphi}^2}{4} < 1, \\ 1 & \text{for } G\dfrac{v^2 - \bar{\varphi}^2}{4} > 1. \end{cases} \tag{19}$$

Expressions (16) and (18) are derived on the assumption that $\kappa\rho \gg 1$.

Expressions (16) and (18) are too complex to deduce the width of the spectral peaks directly from them. However, the combined use of these two expressions makes it possible to solve this problem quite simply and elegantly. In fact, it follows from expression (16) that the maximum value of the output intensity at a peak, which occurs at $\bar{\varphi} = 0$, is

$$\langle I_{\text{out}}\rangle_{\max} = 2(v^2G)^{-1/2}\arctan\left[G^{1/2}\tan\left(\frac{v}{2}\right)\right]. \tag{20}$$

Half of this value gives the half-width of the spectral peak measured at 0.5 of its amplitude. Then, according to expression (18), this half-width can be found from the equation

$$\arctan\left[G^{1/2}\tan\left(\frac{v}{2}\right)\right] = \arctan\left[\frac{vG^{1/2}}{1 - G(v^2 - \bar{\varphi}_{1/2}^2)/4}\right] + \delta\pi \tag{21}$$

and it is equal to

$$\bar{\varphi}_{1/2} = \left(\frac{4}{G + v^2}\right)^{1/2}. \tag{22}$$

This formula is analogous to formula (12) and its meaning is obvious.

All these effects have been considered within the geometric-optics framework. How valid is this approach and to what extent does it correspond to real situations? What is the nature of the influence of diffraction? Strangely enough, in this case the phenomenon of diffraction has a positive influence on a nonideal interferometer by improving its quality [5]. In fact, immediately after reflection from a mirror step, the phase front of a reflected wave is also stepped. In the geometric-optics framework this phase front remains stepped irrespective of the distance travelled. However, diffraction 'smooths out' this step. An increase in the distance between the mirrors (optical thickness d) reduces the influence of a step and brings the situation closer to the case of ideally plane mirrors.

4. Ferroelectric phase of a KDP crystal and its spectral transmission in polarised light

Crystals belonging to the KDP group have a layer domain structure in the ferroelectric phase (Fig. 4). This structure forms during cooling of a crystal below the Curie point, which in the case of KDP is 123 K. The domain configuration formed as a result of the phase transition at the Curie point minimises the free energy as a function of temperature, electric field intensity, and mechanical stress. In general, the domain thickness and the dimensions of polydomain twin blocks can vary within wide limits, so that in the case of a specific realisation it is not possible to predict in advance the nature of the modulation of the optical properties by the domain structure. It follows from the symmetry considerations (Curie principle [9]) that the following are always known: the orientation of the domain walls relative to the crystallographic axes, the direction of the polarisation vector, and the type of the crystal symmetry in the ferroelectric phase.

Separate blocks, consisting of domains with mutually parallel walls (Fig. 4), can be distinguished in the domain structure of KDP-type crystals. The orientation of the domain walls is strictly defined: their planes are perpendicular either to the tetragonal X axis or to the tetragonal Y axis [10–12]. As light propagates in a crystal, an optical wave is scattered by alternating domain blocks with two

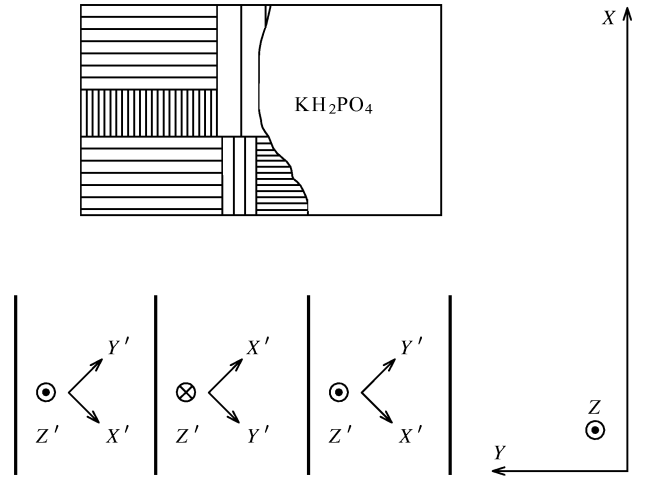

Figure 4. Schematic representation of the domain structure and of the orientation of crystallographic axes in the ferroelectric phase of a KDP crystal. Cooling forms two types of domain blocks: longitudinal and transverse. An enlarged fragment of several transverse domains and of the orientations of the axes in these domains is shown at the bottom of the figure.

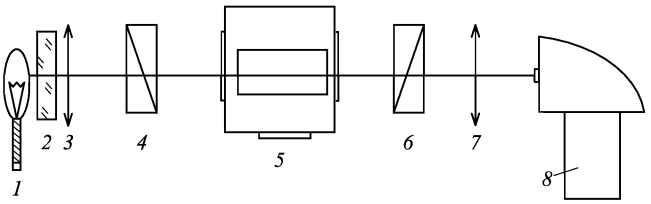

Figure 5. Simplified diagram showing the apparatus used in an investigation of the spectra of a KDP crystal obtained in polarised light: (*1*) tungsten lamp; (*2*) diffuser; (*3, 7*) objectives; (*4*) polariser; (*5*) KDP crystal in a cryostat; (*6*) analyser; (*8*) spectrograph.

types of orientation of the domain walls. An analysis has been made experimentally [6] of light propagating parallel to the planes of the domain walls in blocks of one type (which will be called the longitudinal-domain blocks), but intersecting the walls of domains in blocks of the other type (transverse-domain blocks).

Fig. 5 is a simplified diagram of the apparatus used in an investigation of the transmission spectra. Samples of KDP, in the shape of rectangular parallelepipeds cut along the tetragonal axes, are placed in a liquid-nitrogen cryostat. The dimensions of the domains are altered along the polar Z' axis by a static electric field ($0-4$ kV cm^{-1}). An illumination system (comprising a tungsten lamp, a diffuser, a short-focus lens *3*, and a polariser) forms a diverging beam of white light polarised within $\pm 10°$ relative to the tetragonal X (or Y) axis in the XZ plane. The light transmitted by the crystal and analyser is focused by a lens (*7*) on the slit of a spectrograph. At the output of the spectrograph a two-dimensional spectrum is recorded in terms of two coordinates: the wavelength and the angle. The spectra are recorded on a photographic film or by a photoelectronic system.

Figs. 6 and 7 show photographs of the spectra of polydomain crystals recorded in the $X(Z, Y)XZ$ geometry (the first symbol gives the direction of the wave vector of illuminating radiation at the entry, the symbols in the

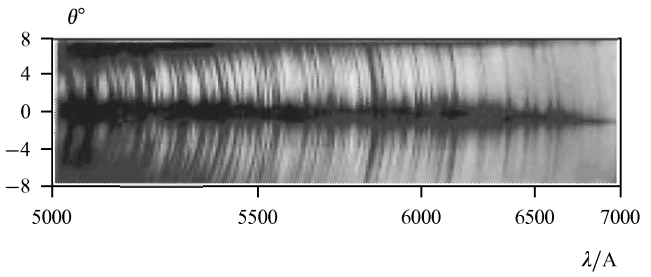

Figure 6. Photograph of the frequency–angle transmission spectrum of a polydomain KDP crystal, 30 mm long.

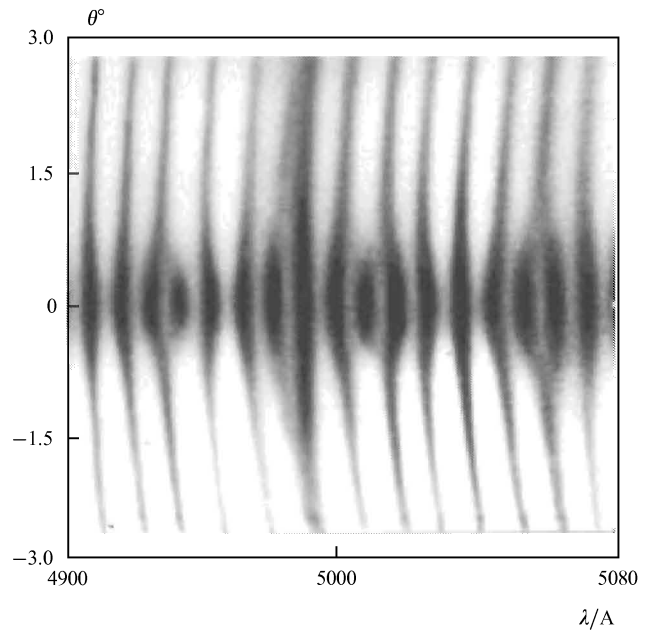

Figure 7. Photograph of a fragment of the frequency–angle transmission spectrum of a crystal, 5 mm long. An interesting feature is the presence of a complex system of fringes near zero value of the angle θ.

parentheses are the directions of the polarisation vector of the radiation at the entry and at the exit, respectively, and the last two symbols define the plane in which the wave vector of the scattered radiation is located, i.e. at the exit). The dependence of the normalised intensity of the transmitted radiation on the wavelength is plotted in Fig. 8.

These transmission spectra of polydomain crystals recorded with crossed polarisers have a number of interesting features.

(1) The intensity of the transmitted light with the orthogonal (relative to the incident light) polarisation depends strongly on the wavelength and angle of observation. The frequency–angle spectrum (Figs 6 and 7) consists of alternating fringes representing the intensity maxima and minima and characterised by a definite curvature. The spectrum of a polydomain crystal obtained for parallel directions of the transmission by the polariser and analyser is complementary relative to the spectrum obtained with crossed polarisers: the intensity maxima are replaced by minima and vice versa.

(2) The spectra are highly sensitive to changes in the domain structure. Variation of an external static electric field, of the thickness of a crystal, or of the region through

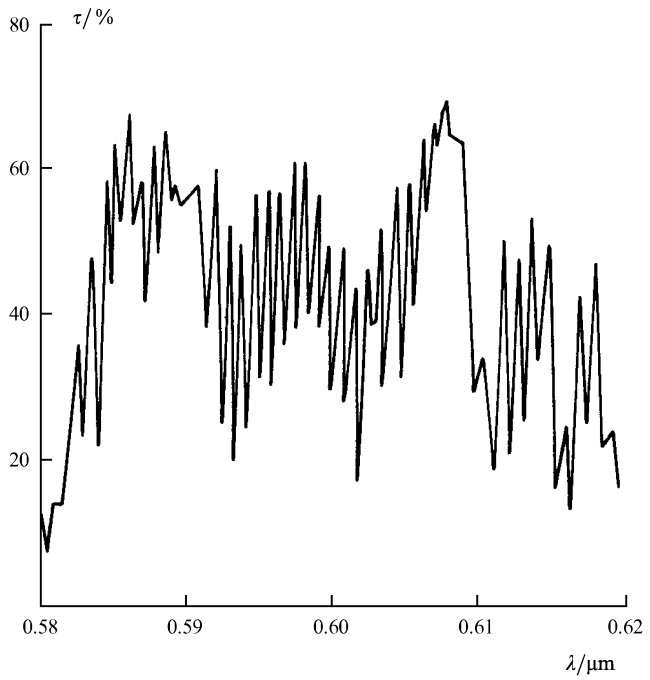

Figure 8. Fragment of the transmission spectrum of a KDP crystal recorded with crossed polarisers. The length of the crystal was 30 mm and the angle θ was 6°.

which light is transmitted alters the domain subsystem and, therefore, the relative intensity and frequency shift of the lines. The curvature of the lines then usually remains constant. When a crystal is converted completely to a single-domain state (by destroying the domain structure) hardly any light with the orthogonal polarisation appears at the crystal exit.

(3) A high degree of depolarisation is observed: the intensity of light at the crystal exit is up to 70% of the incident light intensity.

(4) The frequency–angle spectrum is usually regular and represents an almost equidistant set of fringes. A typical frequency separation between the fringes increases with increase in the wavelength or when the thickness of the sample is reduced.

The history of such spectra is interesting. The subject is fairly old. It has attracted attention in the sixties [13, 14] and in the seventies [15, 16]. Hill et al. [13, 14] were the first to describe modulation of the intensity of monochromatic light transmitted by ferroelectric KDP and DKDP $[K(D_xH_{1-x})_2PO_4]$ crystals. Shinegari and Takagi [15] discovered the frequency modulation of light when they were recording the Raman spectrum of a polydomain KDP crystal. They explained the observed effects by the same mechanism: the interaction of light, represented by the orthogonally polarised modes, as it crosses transversely oriented domain walls of constant thickness. The fullest description of the model is given in Ref. [16].

Characteristic features of the spectra of the polariton scattering of light in KDP were discovered later [17, 18]: the spectra of polydomain samples are considerably different from the spectra of single-domain crystals. The reasons for the difference could be the same as those postulated in Refs [13–16]. This question was tackled in Ref. [6] by investigating the linear transmission spectra of polydomain KDP samples. This was done by the method of recording the frequency–angle transmission spectra, as described above. This method provided detailed information on the characteristics of the transmitted light. As a result, qualitatively new features of the transmission were observed and these did not fit the model developed earlier [13–16]. An analysis of the factors which could give rise to the observed effects led the authors of Ref. [6] to review the proposed mechanism of the formation of the transmission spectra of a polydomain superlattice in a crystal.

The propagation of light in a crystal with a superstructure of the KDP type is still of interest. Objects similar to such crystals are used frequently in various branches of solid-state physics, nonlinear optics, etc. A satisfactory description of the observed effects requires a full understanding of what happens at the simplest level of linear propagation of electromagnetic waves across a superlattice with a symmetry of the type described above. The solution of this problem is tackled in the following sections.

5. Transformation of the polarisation of light by a block of transverse domains

Let us consider the propagation of light in an isolated block of transverse domains. The domains whose axis Z is directed upward will be identified by the index plus, and the adjacent domains with the Z axis directed downward will be identified by the index minus.

If a crystal is illuminated by a plane wave with its front parallel to the entry surface of the crystal and to the walls of transverse domains, a beam of such light splits into two in the crystal: the directions of polarisation for the two beams are orthogonal. They will be labelled as ordinary (o) and extraordinary (e), and one of them (e) is parallel to the Z axis. Let us now assume that the incident plane wave is tilted by an angle θ in a plane perpendicular to the plane of the figure (Fig. 4). The orthogonal polarisation directions are then rotated by an angle $\pm\Delta$ relative to the initial position and the direction of rotation depends on the domain index (plus or minus), so that the direction e makes an angle Δ with the Z axis [16] (Fig. 9).

Let us assume that in some positive Nth domain the complex amplitudes of the o and e waves are O_N and E_N, respectively. It then follows from Fig. 9 that the transition to the negative $(N+1)$th domain is accompanied by the unitary transformation

$$\begin{aligned} O_{N+1} &= O_N \cos(2\Delta) - E_N \exp(\mathrm{i}\delta) \sin(2\Delta), \\ E_{N+1} &= O_N \sin(2\Delta) + E_N \exp(\mathrm{i}\delta) \cos(2\Delta). \end{aligned} \tag{23}$$

Here, the reference phase is that of the (o) wave, which differs from the phase of the extraordinary (e) wave by

$$\delta \cong 2\pi d \frac{n_o - n_e}{\lambda \cos(\theta/n_e)}, \tag{24}$$

where d is the domain thickness and n_α are the refractive indices of the ordinary and extraordinary waves ($\alpha = o, e$).

The next transformation (from a positive to a negative domain) is described by

$$\begin{aligned} O_{N+2} &= O_{N+1} \cos(2\Delta) + E_{N+1} \exp(\mathrm{i}\delta) \sin(2\Delta), \\ E_{N+2} &= -O_{N+1} \sin(2\Delta) + E_{N+1} \exp(\mathrm{i}\delta) \cos(2\Delta), \end{aligned} \tag{25}$$

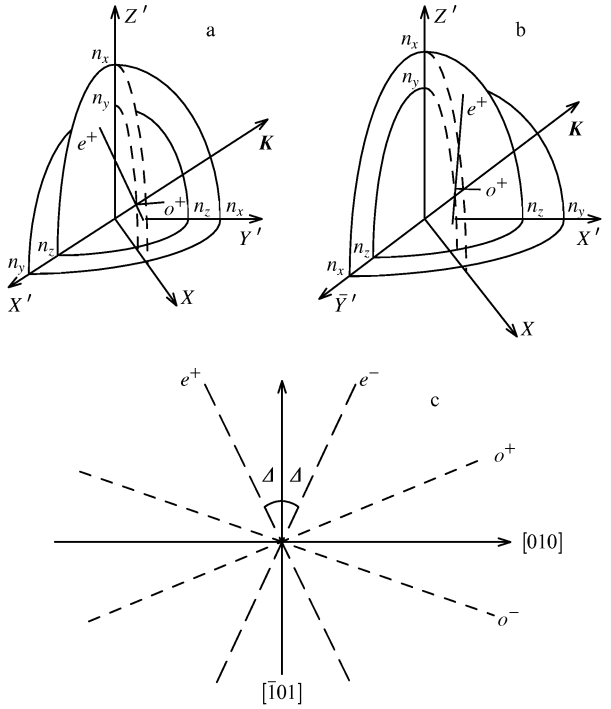

Figure 9. Indicatrices of the refractive indices of opposite positive (+, a) and negative (−, b) domains, and the orientations of the directions of the polarisation of waves propagating in the plane of the tetragonal X and Z axes (c). Here, [010] and [$\bar{1}$01] represent the directions of polarisation in the absence of a domain structure.

i.e. it differs from the transformation (23) in respect of the sign of Δ. Therefore, in general, we have

$$\begin{pmatrix} O_{N+1} \\ E_{N+1} \end{pmatrix} = \begin{pmatrix} \cos(2\Delta) & -\exp(i\delta)\sin(2\Delta) \\ \sin(2\Delta) & \exp(i\delta)\cos(2\Delta) \end{pmatrix} \begin{pmatrix} O_N \\ E_N \end{pmatrix}, \quad \Delta = (-1)^N|\Delta|. \tag{26}$$

These relationships allow us to model the transmission of light across a domain structure and will be used in the subsequent numerical calculations. Since the transformation (26) is unitary and the intensity is normalised, the condition $|O_N|^2 + |E_N|^2 = 1$ should be observed for any value of N.

Estimates show that for $\lambda \approx 0.6$ μm and $T = 100$ K, we have $n_o - n_e \approx 0.04$, and for $\theta = 6$ the angle is $2\Delta \approx 0.3°$. In spite of such a small rotation of the orthogonal directions of the polarisation, the mutual transformation of the o and e waves may be very considerable if the number of domains is large.

If all the transverse-block domains are of the same thickness, the minimum periodicity cell is a component comprising two (one positive and one negative) domains. This component is described by the product of the matrices in expression (26) on the assumption that $N = 1$ and 2:

$$D^{(2)} \equiv \begin{pmatrix} C & \exp(i\delta)S \\ -S & \exp(i\delta)C \end{pmatrix} \begin{pmatrix} C & -\exp(i\delta)S \\ S & \exp(i\delta)C \end{pmatrix} = \begin{pmatrix} C^2 + \exp(i\delta)S^2 & \exp(i\delta)\left(\exp(i\delta) - 1\right)CS \\ \left(\exp(i\delta) - 1\right)CS & \exp(i\delta)\left(\exp(i\delta)C^2 + S^2\right) \end{pmatrix}, \tag{27}$$

where $C \equiv \cos(2\Delta)$, $S \equiv \sin(2\Delta)$.

If $\delta = 0$ or $\delta = 2\pi m$, $m = 0, \pm 1, \pm 2, \ldots$, the ordinary (o) and extraordinary (e) waves do not interact (N is even):

$$D \equiv D^{(N)}D^{(N-2)} \ldots D^{(4)}D^{(2)} = D^{(2)} = \begin{pmatrix} 1 & 0 \\ 0 & 1 \end{pmatrix}, \quad O_N = O_0, \quad E_N = E_0. \tag{28}$$

On the other hand, if $\delta = \pi + 2\pi m$

$$D^{(2)} = \begin{pmatrix} \cos(4\Delta) & \sin(4\Delta) \\ -\sin(4\Delta) & \cos(4\Delta) \end{pmatrix}, \quad D^{(N)} = \begin{pmatrix} \cos(2N\Delta) & \sin(2N\Delta) \\ -\sin(2N\Delta) & \cos(2N\Delta) \end{pmatrix} \tag{29}$$

We shall assume that in the first domain the incident light is polarised along the o direction:

$$\begin{pmatrix} O_0 \\ E_0 \end{pmatrix} = \begin{pmatrix} 1 \\ 0 \end{pmatrix}, \tag{30}$$

so that the interaction of the o and e waves is strongest for the optimal phase $\delta = \pi + 2\pi m$ (for example, if $\delta = \pi$ for $\lambda = 0.6$ μm and $d = 7.5$ μm), as shown in Fig. 10: $O_N = \cos(2N\Delta)$, $E_N = -\sin(2N\Delta)$. The amplitudes of these waves vary harmonically and remain real always. The last condition is satisfied simply if condition (30) is obeyed and $\delta = \pi m$.

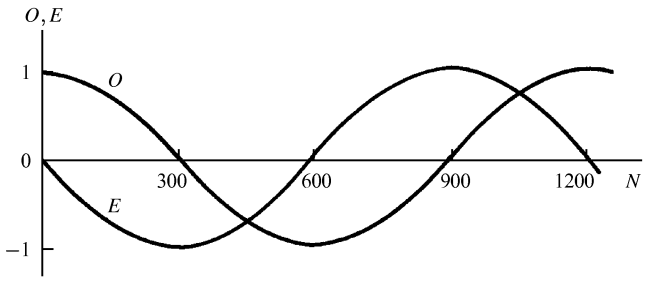

Figure 10. Evolution of the amplitudes O and E of ordinary and extraordinary waves when light propagates across N transverse domain layers, each $d = 7.5$ μm thick when the wavelength of light is $\lambda = 0.6$ μm.

It is evident from Fig. 10 that 300 layer domains can transfer all the energy from the o to the e wave, i.e. this number of domains rotates the plane of polarisation of the initial radiation by 90°. Here is an analogy with Zeno's paradox, as formulated by Peres [19], in the sense that the transformation of light by a large number of identical components is very effective, although the influence of each of these components is slight. The transformation by a large number of components which have little influence can in the limit be more effective than a similar transformation by a small number of components which have a strong influence (for details, see Ref. [19]).

6. Combination of blocks of transverse and longitudinal domains

We shall use the results obtained above for the optimal phase $\delta = \pm\pi$, and consider a somewhat more complex model.

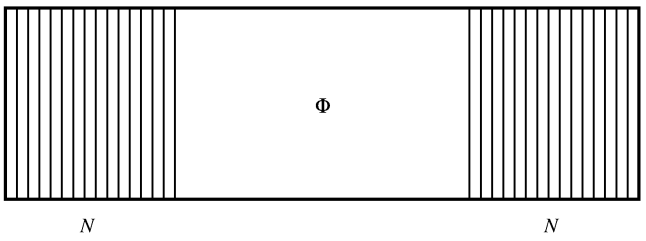

Figure 11.Schematic representation of a domain 'triad' consisting of a phase plate Φ (in particular, this can be a longitudinal-domain block) surrounded by two transverse-domain blocks.

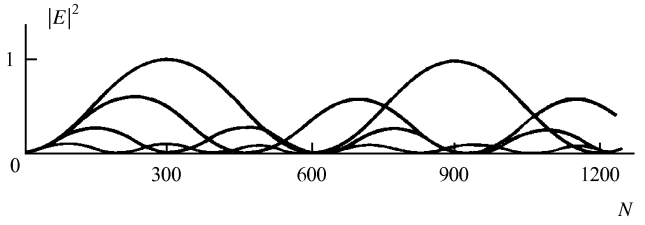

Figure 12. Dependence of the square of the intensity E of an extraordinary wave on the number N of transverse domains of thickness $d = 7.5$ μm, plotted for different phase shifts δ; $\lambda = 0.6$ μm.

Let there be two blocks, each with 150 transverse domains, separated by a phase plate Φ (Fig. 11) which contributes an additional phase φ to the e wave. If $\varphi = 0$ or $2\pi m$, then such a system is simply equivalent to 300 domain layers and the o wave is converted entirely into the e wave. The situation changes radically if $\varphi = (2m + 1)\pi$: for $N = 150$, the sign of the e wave is reversed (see Fig. 10) and we seem to have reached a point $N = 1050$ after which the next 150 layers restore the initial wave amplitudes, i.e. at the point which obeys the condition (30). Therefore, a device shown in Fig. 11 and placed between crossed polarisers, oriented along the o and e directions, is an effective switch or shutter controlled by the phase plate Φ. It should be noted that in the absence of transverse-domain 'end plates', the phase plate Φ could not by itself have any influence on light with the amplitudes described by formula (3), since there would have been no e wave at the entry and no phase corrections to this wave would have had any influence.

A block consisting of longitudinal domains (Fig. 4) can act as the phase plate in the device under consideration. In fact, in the adopted experimental geometry for beams incident at an angle of θ, the longitudinal-domain walls in a block behave as if absent because of the equality of the refractive indices of the adjacent longitudinal domains and because of the identical orientations of the polarisations of the o and e waves.

The phase shift φ in a longitudinal-domain block can be described, under the conditions assumed here, by formula (24) for δ if d is now taken to represent not the thickness of a domain wall, but the length of the whole longitudinal block in the direction of the normal to the entry surface of the crystal. In particular, if this length is 3 mm, then $\varphi = 2\pi m$, where $m = 200$ for $\lambda = 0.6$ μm. The adjacent wavelengths at which we still have $\varphi = 2\pi m$, but $m = 199$ and 201, differ approximately by 3 nm from $\lambda = 0.6$ μm. Therefore, illumination of this device with wide-band white light should apparently give rise to a spectrum of equidistant fringes (lines), similar to that observed experimentally. However, the resonant nature of the interaction of the o and e waves in transverse-domain blocks has been ignored: the condition $\delta = \pm\pi$ for this case is satisfied only at one wavelength and the subsequent maxima in the spectrum are quite far from the first maximum.

The proposed hypothesis was tested by an investigation of the influence of the phase difference δ on the efficiency of the interaction of the o and e waves in a transverse-domain block. The results for the initial state of the polarisation described by formula (30) are presented in Fig. 12.

If δ is arbitrary, then the amplitudes O_N and E_N are complex variables. Fig. 12 gives the dependences of the intensity of the e wave on N for different values of δ. However, the dependence of $|E_N|^2$ on δ for a fixed value of N consists of peaks whose width is approximately 1° of the deviation of the phase δ from the optimal value $\pm 180°$ or ≈ 3 nm in wavelength units relative to $\lambda = 0.6$ μm. The whole system of equidistant lines corresponding to the condition $\varphi = 2\pi m$ should occupy only a narrow spectral interval governed by the width of an interference peak. This is not in agreement with the observation that the lines in the experimental spectra have been recorded throughout the visible range. It is someTimes possible to distinguish several systems of equidistant lines with somewhat different slopes, but in such cases each system occupies a wider spectral interval.

It therefore follows that the influence of the intermediate longitudinal-domain blocks accounts for the appearance of equidistant lines and the separation between these lines agrees (within an order of magnitude) with the experimental observations. The strong shift of the radiation intensity for one polarisation to the other can also be explained on the basis of the real number of domain walls in the investigated samples. However, a further modification of the model is needed and it should soften the resonant nature of the interaction of the waves with orthogonal polarisations in transverse-domain blocks. It is useful to recall here the results given above in connection with the Fabry–Perot interferometer.

7. Influence of the scatter of domain thicknesses

The domains in KDP-type ferroelectric crystals do not form ideal superlattices when they combine to form blocks. Each transverse-domain block may contain domains of different thicknesses. This may broaden the curve representing a resonance of the interaction between light waves with orthogonal polarisations. It is logical to assume that the broadening mechanism is similar to that which applies to interference peaks when random fluctuations of the optical thickness of a Fabry–Perot resonator are taken into account (see Section 3).

Let us now consider a modification of the system discussed in the preceding section and take account of the scatter of the thicknesses in each block relative to an overall average value. Let us assume that the first and third blocks contain 200 domains each and that the average thickness is $\bar{d} = 7.5$ μm, that the thicknesses obey the Gaussian statistics, and that the rms deviation $\sigma \cong 0.185$ μm. A longitudinal-domain block of 3 mm thickness is located between two transverse-domain blocks and plays

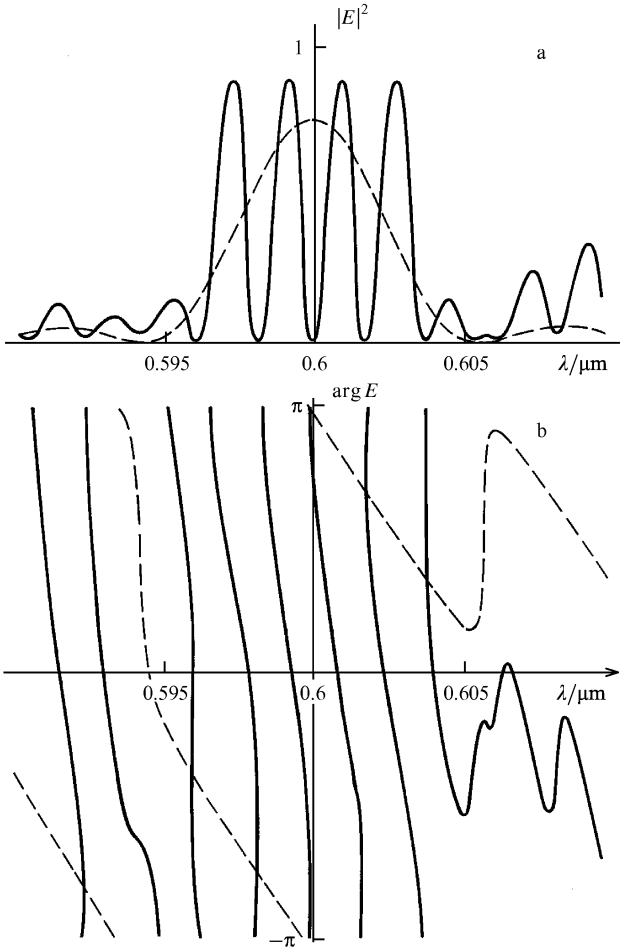

Figure 13. Results of a numerical simulation of a domain triad: square of the the intensity $|E|^2$ (a) and the phase arg E (b) of an extraordinary wave after its passage across the first 200 transverse domain layers (dashed curves) and after passage through the third (last) block, also consisting of 200 transverse domains (continuous curves); $\theta = 6°$, average domain thickness in both transverse blocks $\bar{d}_{1,3} = 7.5$ μm, rms deviation of the thickness of the transverse domains in the blocks $\sigma_{1,3} = 0.185$ μm, length of the longitudinal domain block $d_2 = 3$ mm.

the role of a phase plate. The results of a computer calculation of the spectrum of such a system are presented in Fig. 13. We can see that even relatively small deviations from the domain thickness in the two transverse blocks result in a large number of equidistant lines in the spectrum. In practice, the number of domains, their average thicknesses, the rms deviations, and the nature of the scatter of the domain thicknesses in different blocks may all be different. Moreover, in the course of formation of the scattering spectra we can expect participation not only of three domain blocks, but of a much larger number. Nevertheless, some features of the formation of the spectra can be followed by considering the results of an analysis of this very simple model, which takes account of the effect of the intermediate longitudinal blocks and of some scatter of the domain thicknesses in the transverse blocks.

Let us consider the transformation of the initial state, described by formula (30) in the first transverse-domain block (dashed curves in Fig. 13). The resonance curve $|E_{200}(\lambda)|^2$ has become broadened compared with the case of identical domain thicknesses analysed earlier. In the first approximation this broadening can be calculated in the same way as for random phase shifts in a Fabry–Perot interferometer, which can be done by the use of, for example, expression (9).

Compared with the results of a computer calculation shown in Fig. 13a, an analytic estimate of the broadening of the resonance curve, obtained with the aid of the integral in expression (8), gives somewhat overestimated values. This is because a block of transverse domains of random thickness performs simultaneously the role of a mutual converter of the o–e polarisations and of a phase plate. In fact, if in some domain the conditions for the transformation are optimal (when the thickness d of the domain and the phases of the interacting waves are optimal), then the wall of this domain acts as a polarisation converter. In the opposite case, such a domain performs the function of a passive phase plate. Therefore, during propagation of light across the whole block some of the domains convert actively the o and e waves and some simply contribute additional phase delays (shifts) between them. This interpretation is supported also by the somewhat smaller spacing between the spectral maxima of the whole system (≈2 nm), compared with the estimates that take account of the phase delays only in the second block of longitudinal domains, when the predicted spacing is ≈ 3 nm.

If a transverse-domain block performs active conversion and simultaneously acts as a phase plate, then for certain phases ($\approx \pm\pi$) of the wavelength from the central (peak) value there should be loss of active conversion. This is why in the intervals $\lambda \approx 0.594 - 0.595$ μm and $\lambda \approx 0.605 - 0.606$ μm the $|E_{200}(\lambda)|^2$ resonance curve passes through zero. At these points the phase of the e wave is indeterminate and it may undergo jumps (similar to the jumps that appear as a result of formation of dislocations and branching of interference fringes observed in interferometry). It follows from Fig. 13b that this is precisely the pattern observed in the interval $\lambda \approx 0.605 - 0.606$ μm. The phase jump occurring there is superimposed on the phase modulation contributed by the second (longitudinal-domain) block and the result is the loss of periodicity of the hitherto equidistant spectral maxima (Fig. 13a). Such effects are obviously responsible for the observed deviations of the intermode spacing from the average values in the experimental spectra (see Figs 6–8).

In general, it is possible to predict the appearance of equidistant fringes or lines in a spectrum on the basis of fairly simple considerations. Let us assume that the final block of transverse domains is described by a 22 matrix D. Then the input and output fields entering and leaving this block are related by

$$\begin{pmatrix} O_{out} \\ E_{out} \end{pmatrix} = D \begin{pmatrix} O_{in} \\ E_{in} \end{pmatrix} . \tag{31}$$

The intensity of one of the output polarisations (for example, e) is therefore

$$|E_{out}|^2 = |D_{21} O_{in}|^2 + |D_{22} E_{in}|^2 + 2\mathrm{Re}(D_{21} D_{22}^* O_{in} E_{in}^*), \tag{32}$$

where D_{ij} are the matrix elements of D.

Let us assume that the change in the wavelength λ increases linearly the phase $\varphi_{in} = \arg(E_{in})$ at a rate considerably less than the rate of changes of all the parameters and quantities occurring in expression (32). In reality such 'small-scale' phase modulation occurs specifically in a longitudinal-domain block. It then follows

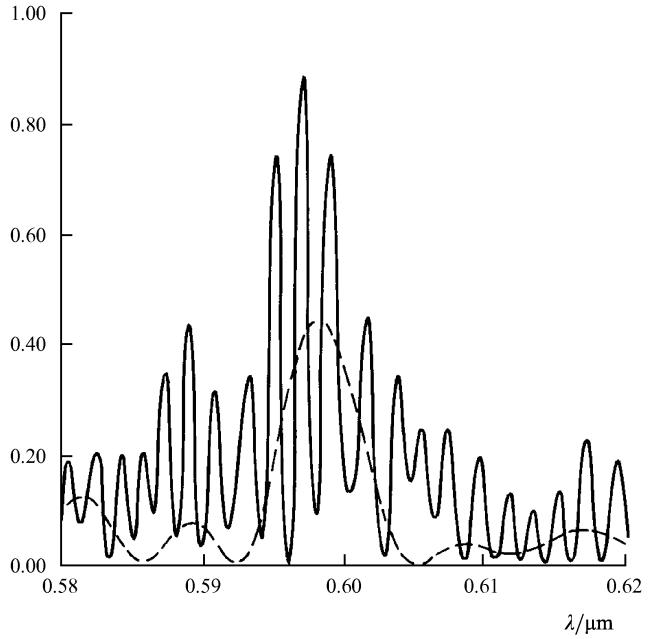

Figure 14. Results of a numerical simulation of the spectrum of a domain triad showing the intensity of an extraordinary wave after passing through a block of the first 200 layers of transverse domains (dashed curve) and the third (last) block, also consisting of 200 transverse domains (continuous curve); $\theta = 6°$, average thickness of domains in transverse blocks $\bar{d}_1 = 7.4$ μm and $\bar{d}_3 = 7.5$ μm, rms deviation of the thickness of domains in transverse blocks $\sigma_1 = 0.8$ μm and $\sigma_3 = 0.74$ μm, length of the longitudinal domain block $d_2 = 3$ mm.

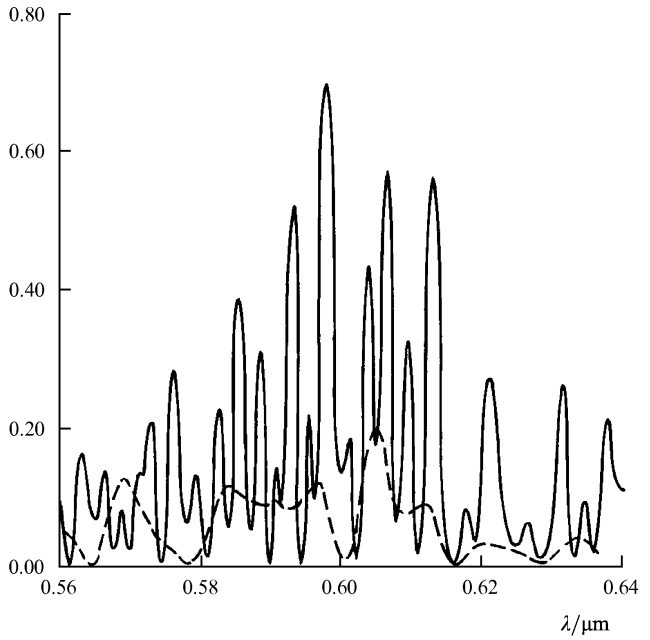

Figure 15. Results of a numerical simulation of the spectrum of a block of transverse domains, showing the intensity of an extraordinary wave after the passage through the first 200 layers of transverse domains (dashed curve) and at the exit from 600 transverse domains (continuous curve); $\theta = 6°$, average domain thickness $\bar{d} = 7.5$ μm, rms deviation of the domain thickness $\sigma = 0.8$ μm.

from expression (32) that a spectrum of equidistant fringes (lines) appears and it has a harmonic envelope in the wavelength interval when only the changes in the phase φ_{in} are significant.

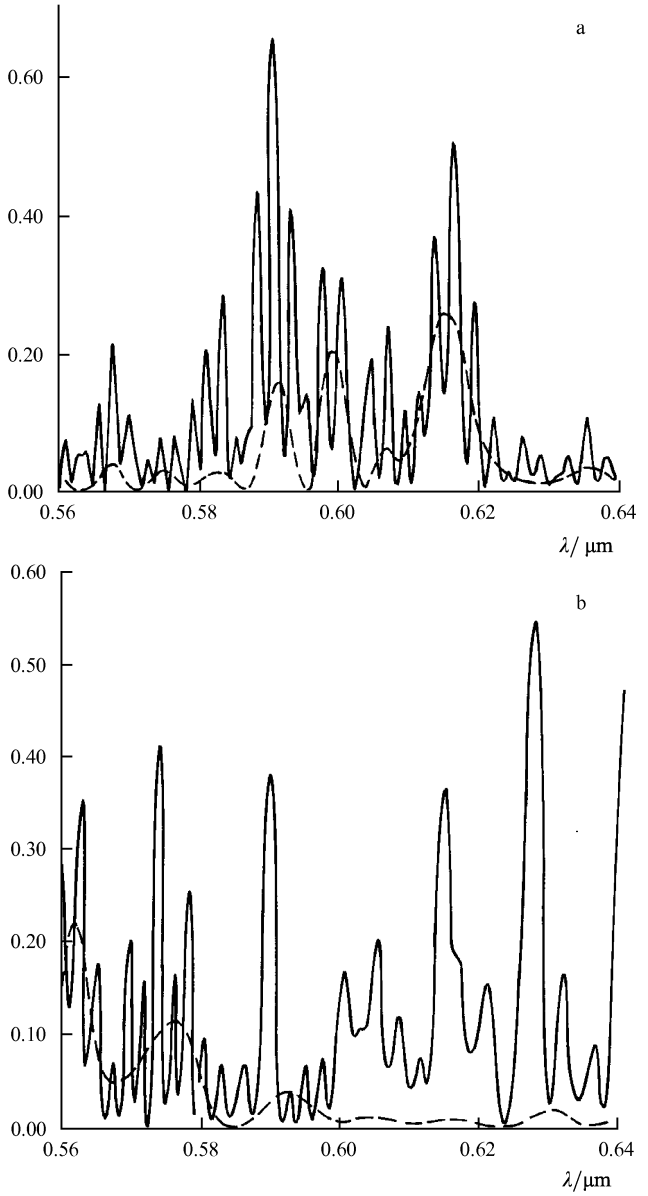

Figure 16. Results of a numerical simulation of the spectra of three blocks of transverse domains (with 200 domains in each), showing the intensity of an extraordinary wave after the passage through the first block (dashed curves) and the third (last) block (continuous curves); $\theta = 6°$; average domain thickness $\bar{d}_1 = 7.6$ μm, $\bar{d}_2 = 10$ μm, $\bar{d}_3 = 7.4$ μm (a), $\bar{d}_1 = 7$ μm, $\bar{d}_2 = 7.9$ μm, $\bar{d}_3 = 7.7$ μm (b); rms deviation of the domain thickness in the blocks $\sigma_1 = \sigma_2 = \sigma_3 = 1$ μm (a, b).

The proposed model is thus capable of explaining some interesting features of the observed experimental spectra. It also makes it possible to formulate approaches to the solution of an incorrectly posed inverse problem: the nature of the spectra can be used to reconstruct the special features of the structure and the statistical characteristics of the domains.

A comparison of the experimental spectra shown in Figs 6–8 with the results of numerical calculations (Fig. 13) leads to the following conclusions:

(1) The presence of equidistant maxima in a wide spectral range is evidence of a wider distribution of the thicknesses of domains in transverse blocks. Fig. 14 is an example of a spectrum calculated for unequal average

values and a large rms scatter of the domain thicknesses in two transverse blocks.

(2) It follows from the results obtained that the condition of equality of the average thicknesses and statistical characteristics in the domains contained in the first and third transverse blocks in such a subsystem is not essential. It is important that their resonance curves should overlap.

(3) In different spectral regions we can expect different 'triads' of domain blocks of this type and the resultant spectrum is a superposition of the spectra of such triads.

Let us go back now to the earlier conclusion that a block of transverse domains performs also active conversion of the polarisation and acts simultaneously as a phase plate. This means that an intermediate block of longitudinal domains is not strictly necessary. In fact, an example of a spectrum formed by *just one* block of transverse domains is shown in Fig. 15. The spectrum is strongly modulated, as also found experimentally. The modulation period is naturally greater than in the case of a triad with transverse–longitudinal–transverse blocks (see Figs 13 and 14). Examples of the spectra formed by three blocks of transverse domains with different average thicknesses are given in Fig. 16. A characteristic feature of these spectra should be stressed once again (see Section 4): the modulation period of the spectral bands increases at long wavelengths (see Fig. 16).

8. Conclusions

Two problems in statistical optics are considered and, in spite of the apparent differences, they are internally related. The 'mystery' of the difficult-to-explain experimental spectra of polydomain KDP crystals might have remained unsolved if the happy analogy with the Fabry–Perot interferometer did not come to mind. What is the usefulness of this approach? The answer is simple: even the model of triads of domain blocks cannot account for the quasiequidistant nature of the fringes or lines unless account is taken of the influence of the stochasticity of the domain thicknesses in transverse blocks, which is similar to the influence of fluctuations of the thickness of a Fabry–Perot interferometer.

Since light has now been shed on the problem in hand, it is useful to consider the promise of further work on polydomain crystals. First, there is an interesting possibility of solving the inverse problem: reconstruction of the domain geometry from the spectra. Second, the authors of Ref. [6] are planning to use these crystals as special nonlinear-optical converters in new experiments on quantum properties of superlattices themselves and of electromagnetic radiation propagating in them. In this connection I would like to mention the recent work of D N Klyshko [20, 21] on the quantisation of fields in such structures.

I hope very much that readers will not be indifferent to these interesting objects for investigation and that this paper will provide the stimulus for the search for intrinsically original methods of using such objects. I am grateful to G Kh Kitaeva, S P Kulik, and A N Penin for providing me with the results of their experiments and for their participation in the work on the second part of this paper (Sections 4–7). I am also indebted to L V Keldysh and D N Klyshko for valuable discussions and comments. The work was supported by a grant from the Russian Fund for Fundamental Research (Project 93-02-14848).

References

1. Zhiglinskii A G, Kuchinskii V V *Real'nyi Interferometr Fabri–Pero* (Real Fabry–Perot Interferometer) (Leningrad: Mashinostroenie, 1983)
2. Dunaev V V, Zhiglinskii A G, Kuchinskii V V *Opt. Spektrosk.* **45** 159 (1978) [*Opt. Spectrosc. (US SR)* **45** 87 (1978)]
3. Sloggett G J *Appl. Opt.* **23** 2427 (1984)
4. Belinskii A V, Chirkin A S *Kvantovaya Elektron. (Moscow)* **13** 906 (1986) [*Sov. J. Quantum Electron.* **16** 593 (1986)]
5. Belinskii A V, Chirkin A S *Kvantovaya Elektron. (Moscow)* **13** 1045 (1986) [*Sov. J. Quantum Electron.* **16** 685 (1986)]
6. Kitaeva G Kh, Kulik S P, Penin A N, Belinsky A V *Phys. Rev. B* **51** 3362 (1995)
7. Born M, Wolf E *Principles of Optics* (Oxford: Pergamon Press, 1964)
8. Tikhonov V I *Statisticheskaya Radiotekhnika* (Statistical Radio Engineering) (Moscow: Radio i Svyaz, 1982) p. 130
9. Jona F, Shirane G *Ferroelectric Crystals* (Oxford: Pergamon Press, 1962)
10. Mitsui T, Furuichi J *Phys. Rev.* **90** 193 (1953)
11. Abbe K *J. Phys. Soc. Jpn.* **56** 757 (1987)
12. Bornarel J *Ferroelectrics* **71** 255 (1987)
13. Hill R M, Ichiki S K *Phys. Rev.* **135** A1640 (1964)
14. Hill R M, Herrmann G F, Ichiki S K *J. Appl. Phys.* **36** 3672 (1965)
15. Shigenari T, Takagi Y *Solid State Commun.* **11** 481 (1972)
16. Takagi Y, Shigenari T *J. Opt Soc. Am.* **63** 995 (1973)
17. Kitaeva G Kh, Kulik S P, Penin A N *Fiz. Tverd. Tela (Leningrad)* **29** 3489 (1987) [*Sov. Phys. Solid State* **29** 2002 (1987)]
18. Kitaeva G Kh, Kulik S P, Penin A N *Fiz. Tverd. Tela (Leningrad)* **34** 3440 (1992) [*Sov. Phys. Solid State* **34** 1841 (1992)]
19. Peres A *Am. J. Phys.* **48** 931 (1980)
20. Klyshko D N *Zh. Eksp. Teor. Fiz.* **104** 2676 (1993) [*J. Exp. Theor. Phys.* **77** 222 (1993)]
21. Klyshko D N *Zh. Eksp. Teor. Fiz.* **105** 1574 (1994) [*J. Exp. Theor. Phys.* **78** 848 (1994)]

Appendix

Calculation of an integral of the type

$$I_n = \int_{-\infty}^{\infty} \frac{\exp(-\alpha x^2)}{\left[\beta^2 + (x+\gamma)^2\right]^n}\,\mathrm{d}x, \tag{A1}$$

where α, β, and γ are real quantities, $\alpha > 0$, and n is a natural number, is required in a range of problems, such as those relating to a spectral analysis. Since the familiar reference handbooks do not give the value of this integral, the results of an analytic calculation are presented below.

Let us begin with the value of this integral when $n = 1$. The integral can then be represented in the form

$$\begin{aligned} I_1 &= (2\beta)^{-1} \int_{-\infty}^{\infty} \frac{\exp(-\alpha x^2)}{\beta + \mathrm{i}(x+\gamma)}\,\mathrm{d}x + \text{c.c.} \\ &= -\beta^{-1}\,\mathrm{Re}\left\{ \mathrm{i} \int_{-\infty}^{\infty} \frac{\exp(-\alpha x^2)}{x + \gamma - \mathrm{i}\beta}\,\mathrm{d}x \right\}, \end{aligned} \tag{A2}$$

where c.c. denotes complex conjugates; i is the imaginary unity; and Re denotes the real part. We shall now rewrite expression (A2) as a sum of two identical terms:

$$I_1 = -(2\beta)^{-1}\,\mathrm{Re}\left\{\mathrm{i}\int_{-\infty}^{\infty}\frac{\exp(-\alpha x^2)}{x+\gamma-\mathrm{i}\beta}\,\mathrm{d}x + \mathrm{i}\int_{-\infty}^{\infty}\frac{\exp(-\alpha x^2)}{-x+\gamma-\mathrm{i}\beta}\,\mathrm{d}x\right\}, \tag{A3}$$

which in its turn becomes

$$I_1 = \beta^{-1}\,\mathrm{Re}\left[(\beta+\mathrm{i}\gamma)\int_{-\infty}^{\infty}\frac{\exp(-\alpha x^2)}{x^2+(\beta+\mathrm{i}\gamma)^2}\,\mathrm{d}x\right], \tag{A4}$$

and the above is the known integral

$$\int_0^{\infty}\frac{\exp(-\alpha x^2)}{x^2+(\beta+\mathrm{i}\gamma)^2}\,\mathrm{d}x = \frac{\pi\exp\left[\alpha(\beta+\mathrm{i}\gamma)^2\right]}{2(\beta+\mathrm{i}\gamma)} \times\left\{1-\mathrm{erf}\left[(\beta+\mathrm{i}\gamma)\sqrt{\alpha}\right]\right\}, \tag{A5}$$

where

$$\mathrm{erf}(u) = 2\pi^{-1/2}\int_0^{u}\exp(-t^2)\,\mathrm{d}t$$

is the probability integral (error function). We thus finally obtain

$$I_1 = \left(\frac{\pi}{\beta}\right)\mathrm{Re}\left[\left\{1-\mathrm{erf}\left[(\beta+\mathrm{i}\gamma)\sqrt{\alpha}\right]\right\}\exp\left[\alpha(\beta+\mathrm{i}\gamma)^2\right]\right]. \tag{A6}$$

The integral I_n can be calculated for an arbitrary n by means of the recurrent relationship

$$I_n = -n^{-1}\,\frac{\mathrm{d}I_{n-1}}{\mathrm{d}p}, \tag{A7}$$

where $p = \beta^2$. For example, we can find I_2 simply by differen-tiating expression (A6) with respect to β^2 and reversing the sign.